Numerical simulations of oblique shock/boundary-layer interaction at a high Reynolds number

By D. Szubert†, I. Jang, G. I. Park AND M. Braza†

This study investigates numerical analysis of the oblique shock/boundary-layer interaction (OSBLI) in a Mach 1.7 flow with a unit Reynolds number of 35 million. Two methods of simulations are performed and compared with an experiment. While two different delayed detached-eddy simulations (DDES) are performed to simulate the full-span geometry, a wall-modeled large-eddy simulation (WM-LES) is carried out to study the physics near the mid-span area. In the experiment, the boundary layer is tripped at the leading edge of the flat plate to ensure fully turbulent boundary layer at the interaction zone. The tripping device in the WM-LES computations was simulated by artificial blowing and suction, while in the DDES simulation turbulence is generated by a Reynolds-Averaged Navier-Stokes (RANS) model and its intensity is adjusted to match the experimental one. Challenges to simulate this test case as well as comparison between the two numerical studies with the experimental results a re highlighted in this paper.

1. Introduction

Research for more effective transport systems and the reduction of emissions, which places severe demands on aircraft velocity and drag reduction, is intense. In order to diminish the shock-induced separation, the boundary layer at the point of interaction should be turbulent. However, the greening of air transport systems means a reduction of drag and losses, which can be obtained by keeping laminar boundary layers on external and internal airplane parts. Therefore, it is very important to develop predictive capabilites of shock-wave/boundary-layer interaction (SBLI) corresponding to new generation of flight conditions and of turbomachinery applications. For example, oblique shock/boundary-layer interaction (OSBLI) has been intensively studied in the European program TFAST (Giepman *et al.* 2014; Szubert *et al.* 2014).

Although computational fluid dynamics (CFD) tools have been frequently used to understand the physical dynamics of OSBLI, the existing computational techniques are in need of further improvement. In their review on the topic, Knight & Degrez (1998) conclude that traditional eddy-viscosity-based Reynolds averaged Navier-Stokes (RANS) approaches may provide unsatisfactory predictions of important features of OSBLI. While interest in higher-fidelity simulations such as DNS or wall-resolved LES is growing, the computational costs quickly become extremely expensive for such complex flows at large Reynolds numbers. Therefore, an optimal compromise between predictive accuracy and computational cost is required to support the design process of supersonic applications. A possible candidate could be a hybrid RANS-LES modeling (for example, delayed-detached eddy simulation (DDES) by Spalart *et al.* 2006). Another candidate is LES

† Institut de Mécanique des Fluides de Toulouse, UMR 5502 (CNRS, INPT, UPS), France

coupled with wall modeling that directly models wall shear stress τ_w and wall heat flux q_w(Kawai & Larsson 2012). Unlike DDES, this wall-modeled LES (WM-LES) resolves the flow all the way down to the wall, but instaneous τ_w and q_w are provided by the wall model as a wall boundary condition.

The objective of this study is to evaluate the performance of DDES and WM-LES in the context of a fully turbulent boundary layer interacting with an oblique shock wave in a supersonic flow. More specifically, the test case treated by the computational techniques is an experimental Mach 1.7 oblique shock wave configuration studied by Giepman *et al.* (2014).

2. Methodology

2.1. *Geometry and conditions*

The geometry of interest for this study is taken from the experiment performed in a transonic/supersonic wind tunnel at the Technical University of Delft (Giepman *et al.* 2014). The cross-sectional area of the test section is 270 mm (height) $\times$ 280 mm (width), and the tunnel was operated at a Mach number of 1.7 with a unit Reynolds number of 35 million. The total pressure and the total temperature were 2.3 bar and 278 K, respectively. The free-stream turbulence level was about 0.5%.

The setup consists of two models, a full-span flat plate with a sharp leading edge ($R \sim 0.15$ mm) and a symmetric partial-span shock generator whose deflection angle is 3°, as shown in Figure 1 (left). The length of the flat plate (L) is 120 mm, and the leading-edge shock of the flat plate itself was very weak ($\theta \sim 0.1°$). The span-wise width of the flat plate (W) is 272 mm, whereas the shock generator has a partial span of 180 mm ($0.66W$). The oblique shock from the shock generator impinges at $x_{LE} = 71$ mm on the flat plate, where x_{LE} is the distance from the leading edge of the flat plate.

In the experiment, the flow is tripped at $x_{LE} = 5$ mm by a zig-zag strip to ensure the presence of a fully turbulent boundary layer entering the shock/boundary-layer interaction. The zig-zag strip is 0.2 mm thick and located in the zone between $x_{LE} = 5$ mm and $x_{LE} = 16$ mm. The span-wise period of the zig-zag shape is 6 mm, and the traversal length of the strip, from the leading edge to the trailing edge of the strip, is 5.8 mm. Without this tripping device, the natural transition is located approximately at $x_{LE} =$ 71 mm.

2.2. *Hybrid RANS-LES modeling (DDES)*

The DDES simulations of the oblique-shock configuration have been performed with the Navier-Stokes Multi-Block (*NSMB*) solver. The NSMB solver is the fruit of a European consortium coordinated by CFS Engineering in Lausanne, Switzerland. NSMB is a structured, finite-volume based, compressible code that includes a variety of efficient high-order numerical schemes and of turbulence modeling closures in the context of LES, URANS and of hybrid turbulence modeling. In this study, a third-order Roe upwind scheme associated with the MUSCL van Leer flux limiter scheme has been used for spatial discretization of the convective fluxes.

The DDES formulation used in this study (Spalart *et al.* 2006) is based, for the unsteady RANS part, on the Edwards-Chandra (Edwards & Chandra 1996) modified Spalart-Allmaras model (Spalart & Allmaras 1994). The Edwards-Chandra modifications result in smooth and faster convergence. A recent application of the DDES method with the NSMB solver can be found in Grossi *et al.* (2014). Implicit time integration us-

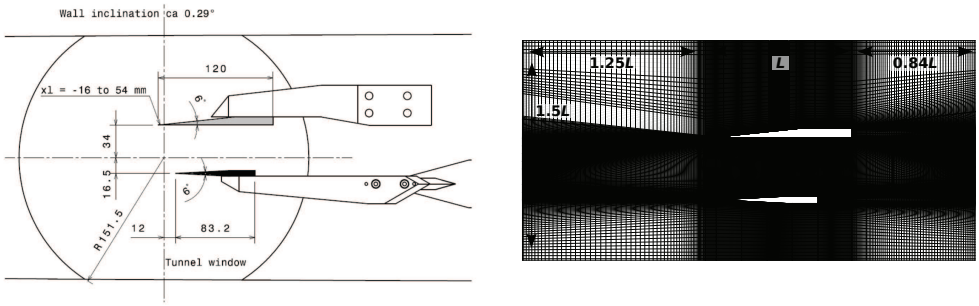

FIGURE 1. Left: Side view of the experimental geometry; right: computational grid for the DDES (mid-span plane) and main dimensions

	N_{total}	Δ_x^+	$\Delta_{y,\min}^+$	Δ_z^+	Δ_x/δ_o	$\Delta_{y,\min}/\delta_o$	Δ_z/δ_o	h_{wm}^+	h_{wm}/δ_o
DDES	31×10^6	296.0	0.04	1006.4	0.42	5.7×10^{-5}	1.42		
WM-LES	4.7×10^6	63.0	8.2	46.3	0.089	0.011	0.065	31.0	0.046

TABLE 1. Grid properties: the grid sizes are normalized by $\delta_{\nu,o}^+$ or δ_o, where the wall viscous unit $\delta_{\nu,o}^+ = \mu_w/(\rho_w u_{\tau,o}) = 1.35 \times 10^{-3}$ mm calculated from the flow values.

ing the dual-time stepping technique has been performed. Typically, 70 inner iterations were necessary for convergence in each time step.

The DDES computations are performed on a full-span domain (272 mm, $W_{DDES}/W = 1$) using symmetry conditions. Two hundred cells are distributed along the span-wise direction. Far-field conditions using the Riemann invariant are imposed at the inlet and outlet, as well as at the top and bottom boundaries. The boundary conditions of the two geometrical elements are adiabatic solid walls. Figure 1 (right) shows a vertical sliced plane of the grid used for the DDES computation. Details of the resolution of this grid are indicated in Table 1. Two DDES calculations are performed. Since previous 2D RANS calculations (Szubert *et al.* 2014) showed an early transition, the first DDES calculation uses no treatments to simulate the effect of the zig-zag tripping in the experiment. A second DDES computation has been carried out by conditionning the flow in a region of short length from the leading edge of the flat plate. This conditioning consists in imposing the turbulent viscosity ν_t to be equal to zero in a defined area of the flow, forcing laminarity in this area, while everywhere else ν_t is evolved from the inlet boundary, based on the experimental value, through the RANS modeling. The rectangle conditioning zone has a height of 1.5 mm from the flat-plate surface and a length of $x_{LE} = 23$ mm $(0.20L)$ from the leading edge, which corresponds to the onset location of the transition in this new simulation. In this case, the development of the turbulent boundary layer is spatially delayed and shows a better agreement with the experiment. This simulation is refered in this study as *transitional DDES*. All the other simulation parameters remained the same as those in the initial DDES computation.

2.3. *Wall-modeled LES*

We use the unstructured compressible LES solver CharLES^x, developed at the Center for Turbulence Research (Bodart & Larsson 2012). CharLES^x utilizes energy-conserving

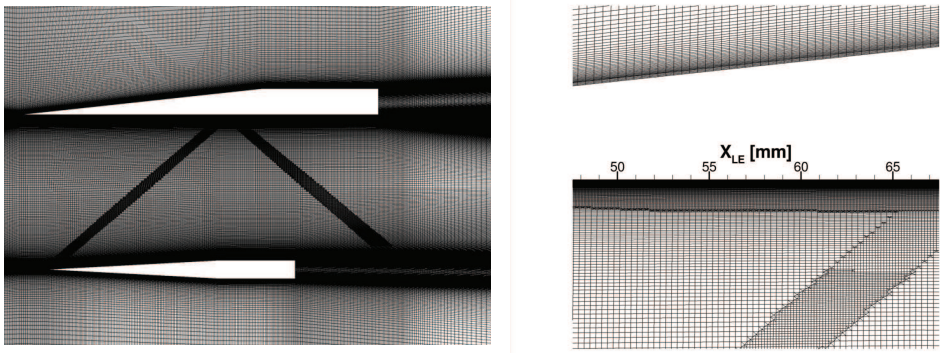

FIGURE 2. WM-LES mesh: (left) computational grids near flat-plate and shock-generator models; (right) enlarged image in the middle of the flat plate

numerics and shows nearly second-order spatial errors for unstructured grids. It also has the ability to detect shocks and switch its central scheme to a 2nd-order ENO method near the detected shocks. For time integration, we use a 3-stage Runge-Kutta method. The Vreman model (Vreman 2004) is applied to model the sub-grid scale motions.

The wall model implemented in CharLES^x was initially proposed by Kawai & Larsson (2012) and generalized by Bodart & Larsson (2012). Since the LES grids do not resolve the inner layer of boundary layers, the wall model calculates the wall shear-stress vector τ_{w} and the wall heat-flux q_{w} and provides them to the LES solver as wall boundary conditions. The model equations are derived from the momentum and energy equations in boundary layers. Based on the assumption of equilibrium boundary layers, all the other terms in the boundary layer equations except the diffusion terms are neglected, which reults in a coupled set of ordinary differential equations. A matching location h_{wm} is specified, at which the solution from the LES grid, (ρ, u, T), is imposed as the upper boundary condition to the wall-model equations. As discussed in Kawai & Larsson (2012), there are at least four LES grid points below h_{wm}.

The WM-LES were performed on a domain whose total stream-wise length is $2.16L$, where again $L = 120$ mm is the stream-wise length of the flat plate. The leading edge of the flat plate is located $0.32L$ from the supersonic inlet, and the domain ends $0.84L$ from the trailing edge of the flat plate. The domain height is the same as the wind-tunnel height of the experiment (0.255 mm). The span-wise domain length ($W_{\text{WM-LES}}$) is 3 mm ($W_{\text{WM-LES}}/W = 0.011$, $W_{\text{WM-LES}}/L = 0.025$), and periodic boundary conditions are used. The LES grids are locally refined in the flat-plate boundary layer (0 mm $\leq x_{LE} \leq$ 98.25 mm) and near the shocks. Figure 2 shows a close view of the refined mesh. The resolutions of the LES mesh and the matching location height are indicated in Table 1.

The inflow turbulence is generated by the digitally filtered synthetic turbulence by Touber & Sandham (2008) that is implemented in CharLES^x by Bermejo-Moreno *et al.* (2011). The turbulent intensity of the synthesized turbulence is the same as the experiment. A supersonic characteristic boundary condition is imposed at the outlet boundary. The top and bottom boundaries are slip walls, and thus the flow cannot penetrate through those boundaries. The walls of the flat plate and the shock generator are adiabatic. As previously explained, periodic boundary conditions are enforced in the span-wise direction. The flow field is initialized with a steady-state two-dimensional RANS simulation

result, and the simulation runs for a total run time of $634.3T$ (statistics are taken after $422.9T$), where the time sacle T is defined as $T = \delta_o/u_\infty$.

In the experiment, the flow is tripped at the leading edge by a 0.2 mm thick zig-zag strip to generate a fully turbulent boundary layer. In the WM-LES simulation, turbulence is triggered by blowing-and-suction at the wall. Following Huai *et al.* (1997), the blowing and suction boundary condition has the form of the following oblique-wave function,

$$v(x,z,t) = A_1 f(x)\sin(\omega t) + A_2 f(x) g(z) \sin\left(\frac{\omega}{2}t\right). \tag{2.1}$$

The stream-wise mode $f(x)$ is taken from Fasel & Konzelmann (1990), which is given as

$$\begin{aligned} |f(x)| =& 15.1875\zeta^5 - 35.4375\zeta^4 + 20.25\zeta^3, \\ \text{where } \zeta =& \begin{cases} \frac{x-x_s}{2(x_e-x_s)} & \text{for } x_s \le x \le x_m \\ \frac{x_e-x}{2(x_e-x_s)} & \text{for } x_m \le x \le x_e \end{cases}, \end{aligned} \tag{2.2}$$

and the stream-wise coordiates are $x_s = 7.75$ mm, $x_m = 10.5$ mm, and $x_e = 13.25$ mm from the leading edge of the flat plate. The span-wise mode $g(z)$ is defined as $g(z) = \cos(2\pi z/\lambda_z)$. The wave amplitudes are $A_1 = 0.05U_\infty$ and $A_2 = 0.005U_\infty$. In order to obtain a strong response from the blowing-and-suction boundary condition similar to that in the experimental tripping device, the amplitudes A_1 and A_2 are taken to be much greater than those in the H-type transition studies such as Fasel & Konzelmann (1990), Huai *et al.* (1997), and Sayadi *et al.* (2013). The non-dimensional frequency is $F = 5.42 \times 10^{-4}$, where $F = 2\pi\omega\left({}^{\mu_\infty}/_{\rho_\infty U_\infty^2}\right)$, and the span-wise wavelengh λ_z is 3 mm. Since the other frequencies and magnitudes except the given values are not investigated in this study, the effects of different blowing-and-suction parameters are not clear.

3. Results and discussion

Since turbulence is generated by mechanisms different from those in the experiment, it is important to verify that the upstream laminar boundary layer becomes the equilibrium turbulent boundary layer by the time when it reaches the shock impingement point ($x_{LE} = 71$ mm). In order to compare compressible results against incompressible skin-friction correlations, we transformed the skin-friction coefficient by using the van Driest II transformation (van Driest 1951), which is given as

$$C_{f_{VD}} = \frac{\overline{T_w}/T_\infty - 1}{\arcsin^2\psi} C_f, \quad \psi = \frac{\overline{T_w}/T_\infty - 1}{\sqrt{\overline{T_w}/T_\infty\left(\overline{T_w}/T_\infty - 1\right)}}, \quad \mathrm{Re}_{\theta VD} = \frac{\mu_\infty}{\overline{\mu_w}}\mathrm{Re}_\theta. \tag{3.1}$$

The transformed skin-friction coefficient $C_{f_{VD}}$ is then compared with the Blasius laminar profile and the turbulent theory by von Kármán & Shoenherr (Hopkins & Inouye 1971) given as

$$C_{f_B} = 0.26\mathrm{Re}_\theta^{-0.25} \tag{3.2}$$

and

$$C_{f_{KS}} = \left\{17.08\left(\log_{10}\mathrm{Re}_\theta\right)^2 + 25.11\log_{10}\mathrm{Re}_\theta + 6.012\right\}^{-1}. \tag{3.3}$$

Figure 3 shows the skin-friction coefficients in the simulations compared with the two theoretical profiles. The WM-LES data are taken in the region of $x_{LE} = 18$ - 65 mm. The turbulent boundary layer in WM-LES matches very well with the theoretical curve after it becomes turbulent ($\mathrm{Re}_\theta > 1000$) by using blowing and suction. The DDES result first

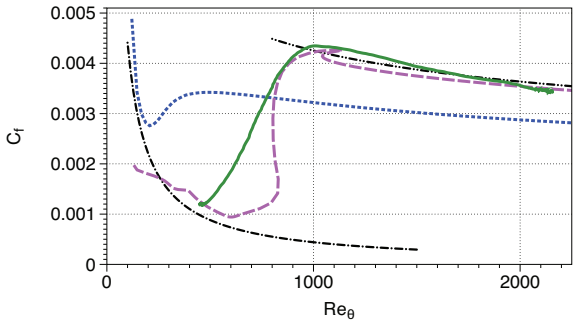

FIGURE 3. Upstream skin-friction coefficient distribution: Blasius, von Kárman & Shoenherr, DDES, DDES (transitional), WM-LES

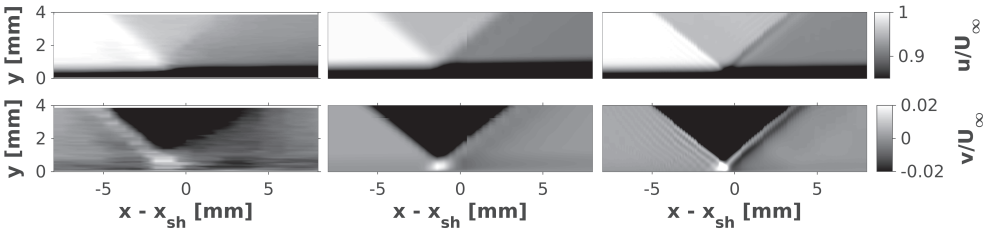

FIGURE 4. Comparison of normalized cross and streamwise velocity fields in the SBLI region. Left: experiment; middle: DDES; right: WM-LES.

follows the laminar Blasius profile but undergoes transition to turbulence much earlier than WM-LES. After transition, a significant discrepancy between the DDES and the theoretical skin friction for equilibrium boundary layers is observed. With regard to the transitional DDES, the boundary layer is not free to develop in terms of turbulence, which explains the unusual aspect of the curve up to $\mathrm{Re}_\theta < 1150$. Downstream of this location, outside the conditioning area, the skin-friction coefficient confirms that the boundary layer is fully turbulent, matching well with the theoretical and the WM-LES values, which endorses the use of the boundary-layer conditioning. A qualitative comparison of the stream-wise and wall-normal velocity fields are provided in Figure 4. In the figures, the horizontal axis is the distance from the shock impingement point x_{sh}, where x_{sh} is 71 mm from the leading edge of the flat plate. The vertical axis of the figures is the distance from the flat plate. The averaged fields from DDES and WM-LES are compared with the steady experimental PIV measurements. Despite extra waves generated by the WM-LES and visible in the v/U_∞ field from the SBLI, the two numerical methods compare well with the experiment.

In Figure 5, the mean stream-wise velocity profiles of the boundary-layer, around x_{sh}, are provided at eight different stream-wise locations and allow a more detailed comparison. The velocity profiles are normalized by the corresponding local free-stream velocities in the experiment at each location. In the DDES case, the mean stream-wise velocity is underestimated compared to the experiment, which can be understood as an overestimation of the development of the turbulence in the boundary layer. The Spalart-Allmaras model induces a quasi-instantaneous laminar-turbulent transition from the leading edge in the RANS layer (Figure 3), while in the experiment, the transition is triggered in

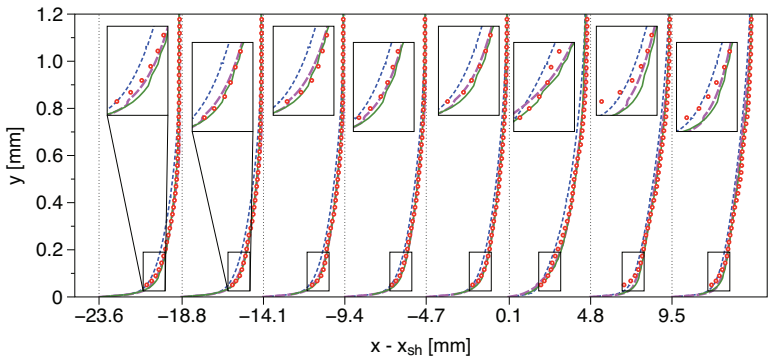

FIGURE 5. Velocity profiles at 8 stream-wise locations: normalized by experimental u_∞ at each location: ····· DDES, - - - - DDES (transitional), —— WM-LES, ○ experiment

the zone of x_{LE} = 5 - 16 mm by the zig-zag tripping. The result of the transitional DDES matches better with the experiment by using the conditioning of the boundary layer, which delays its development to the turbulent state, until the flow approaches the interaction zone where the decrease in velocity observed in the experiment is underpredicted. WM-LES profiles matches well with the experiment, especially in the upstream and downstream directions of the OSBLI zone. In the interaction zone ($x - x_{sh}$ = 0.1 and 4.8 mm), however, there are noticeable discrepancies from the experiment, similar to the transitional DDES. Since an equilibrium WM-LES formulation is used in this study, non-equilibrium effects such as strong pressure gradient and flow recirculation cannot be achieved in the wall model. Dawson *et al.* (2013) also observed poor predictions through interaction in their study of a supersonic compression ramp using a WM-LES. By investigating the magnitude of each term in a wall-resolved LES in the same configurations, they concluded that the convective and pressure gradient terms are dominant in near interaction zone. However, previous attempts to include dominant terms measured at the matching location (h_{wm}) in the equilibirum formulation such as that by Hickel *et al.* (2012) not only had difficulties in showing a satisfactory result but also suffered from numerical stability problems. As the flow goes downstream of the interaction and recovers equilibrium behavior, the WM-LES profiles is getting close to the experiment. Therefore, it may be necessary to solve the full non-equilibrium equations in the wall model. However, the accuracy of the PIV measurements in the SBLI region is reduced compared to that of the other regions of the boundary layer.

Figure 6 shows the distributions of boundary-layer thickness (δ_{99}), displacement thickness (δ^*), momentum thickness (θ), and shape factor ($H = \delta^*/\theta$) as a function of x_{LE}. For δ_{99}, DDES and WM-LES match relatively well with the upstream of the SBLI, given the fact that in general δ_{99} cannot be accurately defined for such complex flows. For δ^* and θ, however, the DDES slightly overestimates the integral values, which confirms the remarks of the previous paragraph: without any conditioning, the DDES generates an early development of the turbulent boundary layer compared to the experiment. This can be corrected by imposing the transition at x_{LE} = 23 mm, as explained above. In this case, the development of the boundary layer is delayed, as shown in all the graphs, and the integral values downstream of the transition location get closer to the WM-LES and the experiment. In the interaction zone, none of the numerical methods can predict

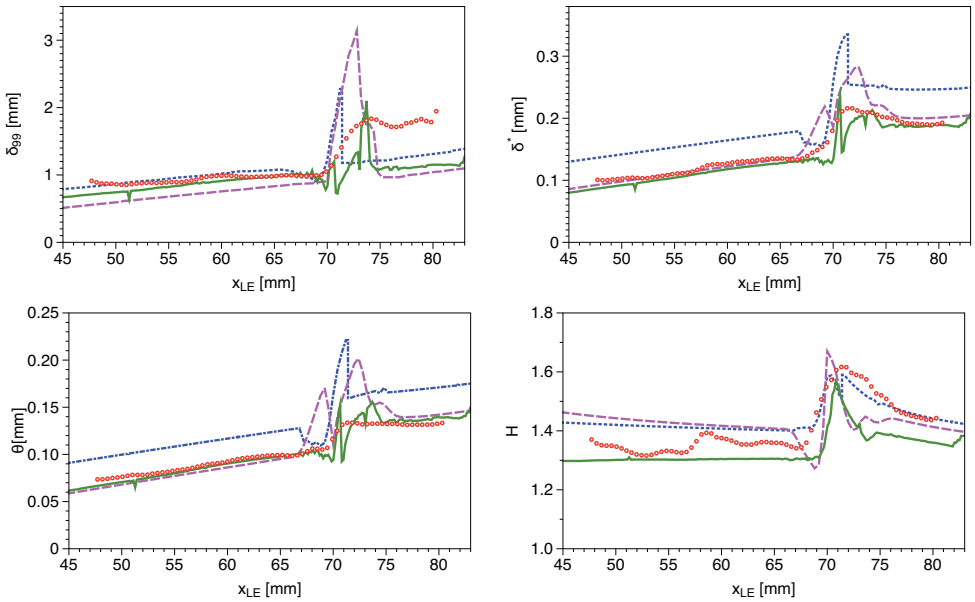

FIGURE 6. Boundary layer thicknesses: (top left) 99% boundary-layer thickness (δ_{99}) (top right) displacement thickness (δ^*) (bottom left) momentum thickness (θ) (bottom right) shape factor (H); ····· DDES, - - - DDES (transitional), —— WM-LES, ○ experiment

accurately the quantities. In the downstream of the interaction, the WM-LES approaches the experimental values as well as the transitional DDES, as observed in Figure 5. For the shape factor (H), both the transitional DDES and the WM-LES are reasonably close to the experimental value in $x_{LE} < x_{sh}$. In the interaction zone, the transitional DDES and the WM-LES follows the general trend of the experiment but shows noticeable discrepancies from the experiment. In the downstream of the interaction zone, the transitional DDES shows a better agreement with the experiment. Interestingly, the DDES results are closer to the experiment for $x_{LE} \geq x_{sh}$ than for the other two calculations despite its poor predictions of the upstream flow for the other quantities without conditioning. We briefly recall that the PIV measurements are less accurate in the SBLI region than in the other regions of the boundary layer.

4. Concluding remarks and future work

Two different simulation tools (a hybrid RANS-LES (DDES) and an equilibrium WM-LES) are used to predict an OSBLI problem in a Mach 1.7 flow. The flow is tripped very close to the leading edge in the experiment to insure a turbulent interaction, and both numerical approaches use different techniques to simulate the tripped fully turbulent boundary layer. All calculations compare reasonably well with the overall features in the experiment. While the results of the DDES modeling show an overestimation of the integral values of the boundary layer, the transitional DDES and the WM-LES match well with the boundary-layer characteristics found in the experiment for the supersonic equilibrium flows. The results of DDES show an overestimation of the development of the boundary layer compared to the reference results. Therefore, DDES requires a pre-

conditioning of the upstream boundary layer in an analogy with the WM-LES that used blowing and suction for the tripping in the experiment.

Despite the good agreement with the experiment in the upstream equilibrium boundary layer, all the numerical methods show discrepancies in the zone of the OSBLI. Strong pressure gradient and complex flow features near the wall at the interaction cannot be represented in the numerical methods. Similar to the findings of Dawson *et al.* (2013), the WM-LES needs to incorporate non-equilibirum dynamics for strong non-equilibrium regions. A possible future approach is the non-equilibirum WM-LES formulation suggested by Park & Moin (2014), which uses a full non-equilibrium formulation to calculate the transient wall shear stress τ_w and heat flux q_w. However, even the full non-equilibrium WM-LES formulation cannot guarantees a more exact prediction in some strongly separated flows (see Balakumar *et al.* (2014), this volume).

Moreover, in the context of the original TFAST project, a study of the laminar-turbulent transition location can be carried out to analyze the effects of this location on the SBLI and the downstream shear layer properties such as characteristic sizes, coefficients, unsteadinesses.

Acknowledgments

The authors acknowledge use of computational resources from the Certainty cluster awarded by the National Science Foundation to CTR. The authors acknowledge underwrote the French Supercomputing Centers CINES and CALMIP for the CPU allocation that permitted the DDES study, Y. Hoarau (ICUBE - Université de Strasbourg, France) and Technical University of Delft (R. Giepman, F. Schrijer, B. van Oudheusden) for providing the experimental results. This study has been carried out in the context of the TFAST European programme (Transition Location Effect on Shock Wave Boundary Layer Interaction).

REFERENCES

Balakumar, P., Park, G.I. & Pierce, B. 2014 DNS, LES, and wall-modeled LES of separating flow over periodic hills. *Proceedings of the Summer Program,* Center for Turbulence Research, Stanford University, pp. 407–415.

Bermejo-Moreno, I., Larsson, J., Campo, L., Bodart, J., Vicquelin, R., Helmer, D. & Eaton, J. 2011 Wall-modeled large eddy simulation of shock/turbulent boundary-layer interaction in a duct. *Annual Research Briefs*, Center for Turbulence Research, Stanford University, pp. 49–62.

Bodart, J. & Larsson, J. 2012 Wall-modeled large eddy simulation of the Mcdonnell-Douglas 30p/30n high-lift airfoil in near-stall conditions. In *30th AIAA Applied Aerodynamics Conference*.

Dawson, D. M., Bodart, J. & Lele, S. K. 2013 Assessment of wall-modeled large eddy simulation for supersonic compression ramp flows. In *49th AIAA/ASME/SAE/ASEE Joint Propulsion Conference*.

van Driest, E. R. 1951 Turbulent boundary layer in compressible fluids. *J. Aeronaut. Sci.* **18**, 145–160.

Edwards, J. R. & Chandra, S. 1996 Comparison of eddy viscosity-transport turbulence models for three-dimensional, shock-separated flowfields. *AIAA J.* **34**, 756–763.

Fasel, H. & Konzelmann, U. 1990 Non-parallel stability of a flat-plate boundary layer using the complete Navier–Stokes equations. *J. Fluid Mech.* **221**, 311–347.

Giepman, R., Schrijer, F. & van Oudheusden, B. 2014 High-resolution piv measurements of a transitional shock wave-boundary layer interaction. In *44th AIAA Fluid Dynamics Conference*.

Grossi, F., Braza, M. & Hoarau, Y. 2014 Prediction of transonic buffet by delayed detached-eddy simulation. *AIAA J.* **52**, 2300–2312.

Hickel, S., Touber, E., Bodart, J. & Larsson, J. 2012 A parametrized non-equilibrium wall-model for large-eddy simulations. *Proceedings of the Summer Program,* Center for Turbulence Research, Stanford University, pp. 127–136.

Hopkins, E. J. & Inouye, M. 1971 An evaluation of theories for predicting turbulent skin friction and heat transfer on at plates at supersonic and hypersonic mach numbers. *AIAA J.* **9**, 993–1003.

Huai, X., Joslin, R. & Piomelli, U. 1997 Large-eddy simulation of transition to turbulence in boundary layers. *Theor. Comput. Fluid Dyn.* **9**, 149–163.

Kawai, S. & Larsson, J. 2012 Wall-modeling in large eddy simulation: Length scales, grid resolution, and accuracy. *Physics of Fluids* **24**, 015105.

Knight, D. D. & Degrez, G. 1998 *Shock wave boundary layer interactions in high mach number flows: a critical survey of current numerical prediction capabilities.* AGARD Advisory Report no. 287.

Park, G. I. & Moin, P. 2014 An improved dynamic non-equilibrium wall-model for large eddy simulation. *Phys. Fluids* **26**, 015108.

Sayadi, T., Hamman, C. W. & Moin, P. 2013 Direct numerical simulation of complete h-type and k-type transitions with implications for the dynamics of turbulent boundary layers. *J. Fluid Mech.* **724**, 480–509.

Spalart, P. R. & Allmaras, S. R. 1994 A one-equation turbulence model for aerodynamic flows. *La Recherche Aérospatiale* **1**, 5–21.

Spalart, P. R., Deck, S., Shur, M. L., Squires, K. D., Strelets, M. K. & Travin, A. 2006 A new version of detached-eddy simulation, resistant to ambiguous grid densities. *Theor. Comput. Fluid Dyn.*, 181–195.

Szubert, D., Ashton, N., van Veen, W., Grossi, F., Hoarau, Y., Braza, M., Giepman4, R., Schrijer, F. & van Oudheusden, B. 2014 Physics and modelling of the transonic and supersonic shock wave boundary layer interaction of oblique and normal shock at high Reynolds number. In *10th International ERCOFTAC Symposium on Engineering Turbulence Modelling and Measurements*.

Touber, E. & Sandham, N. D. 2008 Oblique shock impinging on a turbulent boundary layer: Low-frequency mechanisms. In *38th AIAA Fluid Dynamics Conference and Exhibit*.

Vreman, A. 2004 An eddy-viscosity subgrid-scale model for turbulent shear flow: Algebraic theory and applications. *Phys. Fluids* **16**, 3670–3681.